

# EFFICIENT AND SCALABLE QUANTUM WALK ALGORITHMS VIA THE QUANTUM FOURIER TRANSFORM

ASIF SHAKEEL

**ABSTRACT.** Quantum walks (QWs) are of interest as examples of uniquely quantum behavior and are applicable in a variety of quantum search and simulation models. Implementing QWs on quantum devices is useful from both points of view. We describe a prototype one-dimensional discrete time QW algorithm that economizes resources required in its implementation. Our algorithm needs only a single shift (increment) operation. It also allows complete flexibility in choosing the shift circuit, a resource intensive part of QW implementations. We implement the shift using the quantum Fourier transform (QFT), yielding, to date, the most efficient and scalable, quadratic size, linear depth circuit for the basic QW. This is desirable for Noisy Intermediate-Scale Quantum (NISQ) devices, in which fewer computations implies faster execution and reduced effects of noise and decoherence. As the QFT diagonalizes unitary circulant matrices, we generalize the shift in the basic QW to introduce spatial convolutions in the QW. We demonstrate our basic QW algorithm using the QFT based shift by running it on publicly accessible IBM quantum computers.

## 1. INTRODUCTION

Quantum walks (QWs) exhibit properties that are fundamentally quantum mechanical, serving to demonstrate in their most basic form, walk patterns that are unachievable by classical random walks. In their sophisticated configurations, they appear in applications in areas as widely apart as quantum simulation models [1, 2] and quantum search algorithms [3]. QWs have been experimentally realized on different physical systems [4, 5]. The reader is referred to [6] for a comprehensive review of QWs. With the public availability of quantum computers, quantum algorithms can be tested and their resource requirements and performance examined. In the current era of Noisy Intermediate-Scale Quantum (NISQ) [7] devices, decoherence and noise may severely degrade the performance of a quantum algorithm implemented on a device, negating any gains to be had from a using a quantum algorithm over a classical one. As a consequence, the issue of resource use in implementation deserves consideration. In this paper we develop a computational description of a one-dimensional discrete time QW that turns into a flexible, scalable and highly efficient implementation in terms of circuit size and depth.<sup>1</sup> It also illustrates that partial optimizations of an algorithm can be done mathematically prior to circuit implementation on a quantum device

A basic discrete time QW is specified by a particle walking on a lattice, at each time step moving from its current *site* position to another in its vicinity, and scattering through *self-interaction*. We will, for this paper, consider a one dimensional walk on a finite lattice. The state of the QW is specified by its position and velocity. Taking the lattice to be of size  $N$ ,

---

*E-mail address:* asif.shakeel@gmail.com

<sup>1</sup>The circuit size is the number of at most two-qubit gates used in the circuit. The circuit depth is the longest path length in gates from an input to an output.

the particle's position  $x \in \{0, \dots, N-1\}$  then labels a basis element  $|x\rangle$  of an  $N$ -dimensional *position* Hilbert space. At each time step, the particle can move one lattice position to the "left"  $x \mapsto x-1$ , or to the "right",  $x \mapsto x+1$ , where the addition/subtraction is modulo  $N$ . This directional motion is encoded in a two dimensional *velocity* Hilbert space with basis elements labeled  $|v\rangle$ ,  $v = -1, +1$ , for left and right moving particle respectively. The QW Hilbert space  $\mathcal{H}$  is given as

$$\mathcal{H} = \mathbb{C}^2 \otimes \mathbb{C}^N$$

with basis elements labeled  $|v, x\rangle := |v\rangle \otimes |x\rangle$ . The state of a QW is an element  $\psi \in \mathcal{H}$  of unit norm  $\|\psi\| = 1$ . A QW evolves through two consecutive unitary actions on its state.

- (i) Scattering operation that acts on the velocity space, i.e., is of the form  $S \otimes \mathbb{I}_x$ , where  $S$  is a unitary matrix on  $\mathbb{C}^2$ , the velocity space, typically [8],

$$S = \begin{bmatrix} ie^{i\alpha} \sin \theta & e^{i\alpha} \cos \theta \\ e^{i\alpha} \cos \theta & ie^{i\alpha} \sin \theta \end{bmatrix}.$$

and  $\mathbb{I}_x$  is the identity operator on the position space.

- (ii) Propagation operation that moves the particle in the direction of the velocity,

$$\sigma : |v, x\rangle \mapsto |v, x+v\rangle,$$

where the addition is modulo  $N$ .

Denoting

$$\hat{S} = S \otimes \mathbb{I}_x, \tag{1}$$

a step  $T$  of QW evolution is thus:

$$T = \sigma \hat{S}.$$

This is the model of QW that we are going to be concerned with.

The rest of this paper is organized as follows. In Section 2 we describe our QW algorithm that, for  $n$ -qubit position space, implements the right/left shifts (increment/decrement) in propagation  $\sigma$  by single right shift (increment) and  $2n$  CNOT gates that control the direction. We recall the quantum Fourier transform (QFT) and compare the shift implementation using the QFT with the one based on generalized CNOT gates, common in applications. In Section 3 we introduce the QW whose state, during propagation, evolves through spatial convolution, generalizing the shift. We also describe a strategy for efficient implementation of this family of QWs. In Section 4 we run our basic QW algorithm with QFT based shift on some of the IBM quantum computers for a few lattice sizes and number of steps of evolution, and examine their performances. Section 5 is the conclusion.

## 2. AN ALGORITHM FOR QW

Let us first express the vectors and operators in the natural bases for the position and velocity spaces. Considering the position space by itself, we can use the natural ordering

induced on the basis by values of  $x$  and write  $|x\rangle$  as a coordinate vector

$$|x\rangle = \begin{bmatrix} 0 \\ 0 \\ \vdots \\ \vdots \\ 0 \\ 1 \\ 0 \\ \vdots \\ 0 \end{bmatrix} \begin{matrix} (0) \\ (1) \\ \vdots \\ \vdots \\ \\ (x) \\ \\ \vdots \end{matrix} \quad (2)$$

where the coordinate indices are displayed in parentheses and all the component values are 0, except at the index  $x$ , whose component value is 1. Similarly, for the joint velocity-position space, we write  $|v, x\rangle$  as a coordinate vector of length  $2N$ , with the first  $N$  elements representing positions corresponding to  $v = 0$  and the last  $N$ , those corresponding to  $v = 1$ ,

$$|v, x\rangle = \begin{bmatrix} 0 \\ 0 \\ \vdots \\ \vdots \\ 0 \\ 1 \\ 0 \\ \vdots \\ 0 \end{bmatrix} \begin{matrix} (0) \\ (1) \\ \vdots \\ \vdots \\ \\ (Nv + x) \\ \\ \vdots \end{matrix} .$$

Denote by  $\mathbf{X}$  the right shift on the position space alone (generalizing the symbol for one qubit flip  $X$  gate), which as a matrix in our coordinate representation is the  $N \times N$  matrix

$$\mathbf{X} = \begin{bmatrix} 0 & 0 & 0 & \cdots & 1 \\ 1 & \ddots & \ddots & \ddots & \vdots \\ 0 & \ddots & \ddots & 0 & 0 \\ \vdots & \ddots & 1 & 0 & 0 \\ 0 & \cdots & 0 & 1 & 0 \end{bmatrix} . \quad (3)$$

We may check that  $\mathbf{X} |x\rangle = |x + 1\rangle$ , where  $|x\rangle$  is as in Eq. (2). The matrix for propagation  $\sigma$  on the joint velocity-position space is a controlled shift of position  $|x\rangle$  by velocity  $|v\rangle$ , with  $|v\rangle = | +1\rangle$  affecting the right shift  $\mathbf{X}$  and  $|v\rangle = | -1\rangle$  affecting the left shift  $\mathbf{X}^\top$ . Its matrix is

$$\sigma = \begin{bmatrix} \mathbf{X} & \mathbf{0} \\ \mathbf{0} & \mathbf{X}^\top \end{bmatrix} . \quad (4)$$

where  $\mathbf{0}$  is the matrix of all zeros.

Figure 1 shows the circuit for this description of QW with  $\hat{S}$  followed by  $\sigma$ .

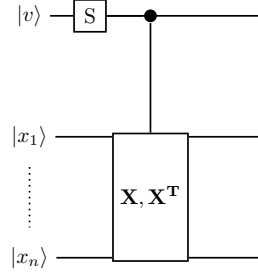


**Figure 1.** A quantum pseudo-circuit for QW. The control  $|v\rangle$  selects  $\mathbf{X}$  or  $\mathbf{X}^\top$

**2.1. Implementing the propagation  $\sigma$ .** The propagation  $\sigma$  in Eq. (4) has a decomposition that we can implement using a single right shift  $\mathbf{X}$  from Eq. (3), as we describe next. Let us first state the definition and a property of Toeplitz matrices, which we then apply toward our decomposition. Recall that a Toeplitz matrix is a square matrix with each descending diagonal from left to right a constant, i.e., a  $N \times N$  matrix  $A$  is Toeplitz if

$$A = \begin{bmatrix} a_0 & a_{-1} & a_{-2} & \cdots & a_{-(N-1)} \\ a_1 & a_0 & a_{-1} & \ddots & \vdots \\ a_2 & a_1 & \ddots & \ddots & a_{-2} \\ \vdots & \ddots & \ddots & \ddots & a_{-1} \\ a_{N-1} & \cdots & a_2 & a_1 & a_0 \end{bmatrix}.$$

for some set of numbers  $\{a_{-(N-1)}, \dots, a_0, \dots, a_{N-1}\}$ . So if we number the rows and columns of  $A$  by  $\{0, \dots, N-1\}$ , then  $A_{i,j} = a_{i-j}$  for all  $0 \leq i, j \leq N-1$ . Also recall the definition of an *exchange* matrix (see Section 1.2.11 of [9]). An exchange matrix is a square matrix with all its entries 0 except those on the anti-diagonal which are all 1. Denote the  $N \times N$  exchange matrix by  $J$ ,

$$J = \begin{bmatrix} 0 & \cdots & 0 & 0 & 1 \\ 0 & \ddots & \ddots & 1 & 0 \\ \vdots & 0 & \ddots & 0 & \vdots \\ 0 & 1 & \ddots & \ddots & 0 \\ 1 & 0 & 0 & \cdots & 0 \end{bmatrix}.$$

The transpose of a Toeplitz matrix can be obtained as follows (Section 4.7 of [9]).

$$A^\top = JAJ.$$

As the shift matrix  $\mathbf{X}$  in Eq. (3) is Toeplitz, by the above property, we can express  $\sigma$  in Eq. (4) as

$$\sigma = \begin{bmatrix} \mathbf{X} & \mathbf{0} \\ \mathbf{0} & J\mathbf{X}J \end{bmatrix} = \begin{bmatrix} \mathbb{I}_N & \mathbf{0} \\ \mathbf{0} & J \end{bmatrix} \begin{bmatrix} \mathbf{X} & \mathbf{0} \\ \mathbf{0} & \mathbf{X} \end{bmatrix} \begin{bmatrix} \mathbb{I}_N & \mathbf{0} \\ \mathbf{0} & J \end{bmatrix}, \quad (5)$$

where  $J$  is the  $N \times N$  exchange matrix and  $\mathbb{I}_N$  is the  $N \times N$  identity matrix. Let us denote the first (and the last) matrix on the right side product decomposition by  $C^v(J)$ ,

$$C^v(J) = \begin{bmatrix} \mathbb{I}_N & \mathbf{0} \\ \mathbf{0} & J \end{bmatrix}. \quad (6)$$

Then  $\sigma$  in Eq. (5) may be written

$$\sigma = C^v(J) (\mathbb{I}_v \otimes \mathbf{X}) C^v(J), \quad (7)$$

where  $\mathbb{I}_v$  is the identity operator on the velocity space.

2.1.1. *Specializing to qubits.* Let us assume further that the lattice is of size  $N = 2^n$  for some finite  $n$ , natural for multi-qubit systems. The binary expansion of the position  $x$

$$x = \sum_{j=0}^{n-1} 2^j x_j, \quad (8)$$

with  $x_j \in \{0, 1\}$ ,  $j \in \{0, \dots, n-1\}$ , gives us a bijective map  $x \leftrightarrow (x_{n-1} \dots x_0)$ . This identifies the bases of position space and of  $n$  qubits:  $|x\rangle \leftrightarrow |x_{n-1} \dots x_0\rangle$ . We also identify the velocity basis states with the usual qubit states as  $|+1\rangle \leftrightarrow |0\rangle$ , and  $|-1\rangle \leftrightarrow |1\rangle$ . Combined, the velocity-position space is thus identified with  $n + 1$  qubits,

$$\begin{aligned} \mathcal{H} &\leftrightarrow \mathbb{C}^{n+1} \\ |+1, x\rangle &\mapsto |0, x_{n-1} \dots x_0\rangle \\ |-1, x\rangle &\mapsto |1, x_{n-1} \dots x_0\rangle \end{aligned}$$

For the rest of this section when we refer to any of the vector spaces, we interpret that as the corresponding multi-qubit space.

Let us turn to the operators. We observe that the exchange matrix  $J$ , in the basis ordering we have, is simply the qubit-wise application of  $X$  to each position qubit  $|x_j\rangle$  (flipping each  $|x_j\rangle$ :  $|0\rangle \rightleftharpoons |1\rangle$ ),

$$J = \bigotimes_{j=1}^n X, \quad (9)$$

where

$$X = \begin{bmatrix} 0 & 1 \\ 1 & 0 \end{bmatrix}.$$

Denote by  $C_j^v(X)$  the  $|v\rangle$ -controlled  $X$  on position qubit  $|x_j\rangle$ , i.e., a CNOT gate controlled by  $|v\rangle$  with target  $|x_j\rangle$ ,

$$C_j^v(X) = \begin{bmatrix} \mathbb{I}_2 & \mathbf{0} \\ \mathbf{0} & X \end{bmatrix},$$

where  $\mathbb{I}_2$  is the  $2 \times 2$  identity matrix and the basis of the space on which  $C_j^v(X)$  acts is  $\{|v, x_j\rangle\}$ . By the expression for  $J$  in Eq. (9), and because  $C_j^v(X)$  and  $C_i^v(X)$  commute for all  $i, j$ , we can write  $C^v(J)$  in eq. (6) as

$$C^v(J) = \prod_{j=1}^n C_j^v(X). \quad (10)$$

This means that  $\sigma$  in eq. (7) can be implemented as in Figure 2.

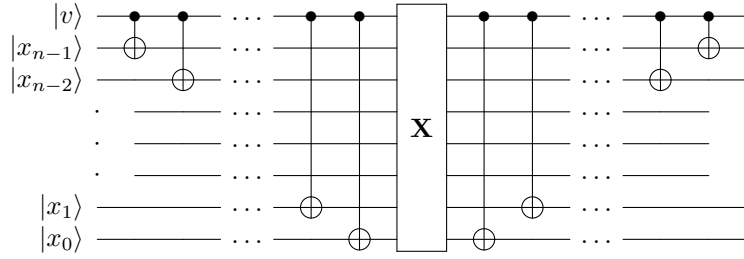


**Figure 2.**  $n$ -qubit  $\sigma$  implementation using a single shift  $\mathbf{X}$

Note that the order in which the CNOT gates are applied on either side of  $\mathbf{X}$  in the circuit of Figure 2 does not matter: they have independent targets and may even be executed in parallel. We have simply chosen one arrangement for the convenience of creating a figure.

By the decomposition just presented, we have taken a substantial step toward decreasing the resources needed for implementation of  $\sigma$ . This is because we use the same shift  $\mathbf{X}$  for increment and decrement, instead of explicitly implementing both a controlled increment and decrement circuit. Note that the left/right direction control is affected by  $C^v(J)$ , while the shift  $\mathbf{X}$  only works as a right shift (increment). This allows us the flexibility of choosing any shift circuit for  $\mathbf{X}$ . To reduce the resources most effectively, we consider the shift implementation that uses the quantum Fourier transform.

**2.2. Quantum Fourier transform based shift implementation.** The quantum Fourier transform (QFT) [11, 12] diagonalizes the shift  $\mathbf{X}$  (see section 4.8 of [9]). Denote the  $N$  dimensional QFT by  $\mathcal{F}$ ,<sup>2</sup>

$$\mathcal{F} : |x\rangle \rightarrow \frac{1}{\sqrt{N}} \sum_{k=0}^{N-1} e^{2\pi i x k / N} |k\rangle,$$

then

$$\mathbf{X} = \mathcal{F}^{-1} \Omega \mathcal{F},$$

where  $\Omega$  is a diagonal phase multiplication matrix

$$\Omega = \begin{bmatrix} 1 & 0 & 0 & \cdots & 0 \\ 0 & \omega & \ddots & \ddots & \vdots \\ 0 & 0 & \omega^2 & 0 & 0 \\ \vdots & \ddots & \ddots & \ddots & 0 \\ 0 & 0 & \cdots & 0 & \omega^{N-1} \end{bmatrix}.$$

This simplifies to a tensor product of  $n$  single qubit phase rotations when  $N = 2^n$ ,

$$\Omega = \begin{bmatrix} 1 & 0 \\ 0 & \omega \end{bmatrix} \otimes \begin{bmatrix} 1 & 0 \\ 0 & \omega^2 \end{bmatrix} \otimes \begin{bmatrix} 1 & 0 \\ 0 & \omega^4 \end{bmatrix} \otimes \cdots \otimes \begin{bmatrix} 1 & 0 \\ 0 & \omega^{2^{n-1}} \end{bmatrix}, \quad (11)$$

where  $\omega = e^{2\pi i / 2^n}$ .

<sup>2</sup>This description of the QFT based shift algorithm was communicated to the author by David Meyer.

The Shor's algorithm [12] for QFT as a circuit is in Figure3.

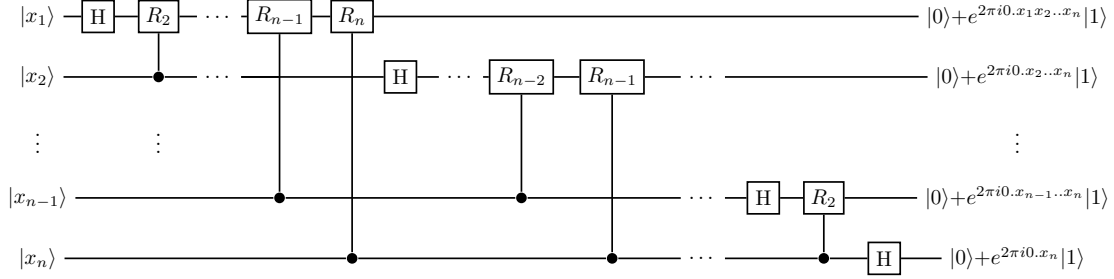


**Figure 3.** Quantum Fourier Transform circuit.

where

$$R_k = \begin{bmatrix} 1 & 0 \\ 0 & e^{2\pi i/2^k} \end{bmatrix}. \quad (12)$$

Note that, strictly, we need to insert  $\lfloor n/2 \rfloor$  swaps (each in turn requiring 3 CNOT gates) at the end of the QFT circuit to get the output ordered correctly. Since we use QFT and the inverse quantum Fourier transform (IQFT) together to achieve the shift  $\mathbf{X}$ , the swaps can be absorbed in  $\Omega$ , by reversing the order of phase rotation operations on qubits. To be precise, we can express  $\Omega$  in eq. (11) in terms of  $R_k$  in eq. (12) above as

$$\Omega = R_n \otimes R_{n-1} \otimes R_{n-2} \otimes \dots \otimes R_1 \quad (13)$$

The swaps in QFT and IQFT can be omitted by replacing  $R_k, k \in \{1, \dots, n\}$ , in the above expression for  $\Omega$  with  $R_{n-k+1}$ .

Let us estimate the number of (at most) two-qubit gates needed for this implementation of  $\mathbf{X}$ . QFT [12] and its inverse each require  $n(n+1)/2$  gates, excluding swaps at the end, which are not needed by the observation above.  $\Omega$  requires  $n$  phase rotations. Thus in total, this implementation of  $\mathbf{X}$  requires  $n^2 + 2n$  gates. The circuit depth is  $n$ . The entire QW implementation requires an additional  $2n$  CNOT gates and a rotation for the scattering. This adds up to a circuit size of  $n^2 + 4n + 1$  and circuit depth of  $3n + 1$ .

**2.2.1. Comparison of QFT based shift implementation with generalized CNOT based implementation.** The right shift  $\mathbf{X}$  can be implemented using generalized CNOT gates, for instance, as in [10]. Implementations of generalized CNOT gates are described in [12, 14, 15], and the circuit symbol for an  $n$ -qubit generalized CNOT gate is shown in Figure 4 below.

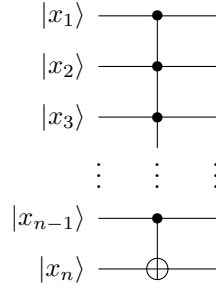


**Figure 4.**  $n$ -qubit generalized CNOT gate

Shift **X** implementation using the generalized CNOT gates is shown in Figure 5 below.

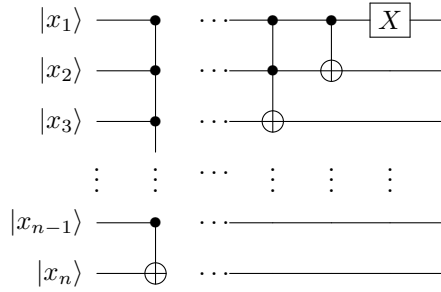


**Figure 5.** Generalized CNOT gate based  $n$ -qubit shift

When  $n = 3$  the generalized CNOT gate is also called the CCNOT gate or the Toffoli gate. For  $n \geq 3$ , a generalized CNOT gate can be implemented [15] by a circuit of size  $2n^2 - 6n + 5$  and depth  $8n - 20$ . The shift circuit above, for  $n \geq 3$ , without any further circuit optimizations that may be possible, therefore, has size  $n(n+1)(2n+1)/3 - 3n(n+1) + 5n = n(2n^2 - 6n + 7)/3$  and depth  $4n(n+1) - 20n + 18 = 2(2n^2 - 8n + 9)$ . Both the circuit size and depth in this shift implementation are an order of  $n$  in magnitude larger than the QFT based shift.

An alternative is to use ancilla qubits and CNOT gates as in [14]. For a  $n \geq 4$  qubit generalized CNOT gate, this would require  $n - 3$  ancilla qubits and  $4(n - 3)$  CCNOT gates, with a circuit depth (in CCNOT gates) of  $4(n - 3)$ . From [15], each CCNOT gate requires 4 (at most) 2-qubit gates. The generalized CNOT then translates to a circuit size of  $20(n - 3)$  in (at most) 2-qubit gates and depth of  $16(n - 3)$ . The  $n - 3$  ancilla qubits can be reused among the generalized CNOT gates of the shift circuit. The shift circuit, for  $n \geq 4$ , without any further circuit optimizations, would then be of size  $10n^2 - 50n + 67$  and of depth  $2(4n^2 - 20n + 27)$ . This, for large  $n$ , is a factor of 5 higher than the QFT based shift in circuit



size and an order of  $n$  in magnitude larger in depth, even without the cost of ancilla qubits, which effectively double the number of required qubits in this circuit implementation.

### 3. QW EVOLUTION WITH SPATIAL CONVOLUTION

QFT, in fact, diagonalizes any unitary circulant matrix (see section 4.8 of [9]), i.e., any convolution matrix. Recall that an  $N \times N$  circulant matrix is a special type of Toeplitz matrix of the form

$$C = \begin{bmatrix} c_0 & c_1 & c_2 & \cdots & c_{N-1} \\ c_{N-1} & c_0 & c_1 & \ddots & \vdots \\ c_{N-2} & c_{N-1} & \ddots & \ddots & c_2 \\ \vdots & \ddots & \ddots & \ddots & c_1 \\ c_1 & \cdots & c_{N-2} & c_{N-1} & c_0 \end{bmatrix}.$$

Instead of the dynamics based on shift  $\mathbf{X}$ , we would like to accomplish the dynamics of QW based on unitary circulant matrices. In this scheme, the state at a site after a time step would depend on the state of the walk at the neighboring sites before the step through a unitary spatial convolution more general than a shift. Let circulant matrices  $C, C'$  determine the dynamics in that the propagation matrix, in the joint velocity-position<sup>3</sup> basis, is

$$\sigma = \begin{bmatrix} C & \mathbf{0} \\ \mathbf{0} & C' \end{bmatrix}. \quad (14)$$

The QW evolution in this setting proceeds as before by scattering the velocity by a unitary matrix  $S$  followed by the propagation above. The evolution of the QW is:

$$T = \sigma \hat{S},$$

where  $\hat{S}$  is as in eq. (1).

Let

$$C = \mathcal{F}^{-1} \Lambda \mathcal{F} = \mathcal{F}^\dagger \Lambda \mathcal{F}$$

where

$$\Lambda = \begin{bmatrix} e^{i\theta_0} & 0 & 0 & \cdots & 0 \\ 0 & e^{i\theta_1} & \ddots & \ddots & \vdots \\ 0 & 0 & e^{i\theta_2} & 0 & 0 \\ \vdots & \ddots & \ddots & \ddots & 0 \\ 0 & 0 & \cdots & 0 & e^{i\theta_{N-1}} \end{bmatrix},$$

and  $\theta_j, j \in \{0, \dots, N-1\}$ , are real. Similarly we have the decomposition

$$C' = \mathcal{F}^\dagger \Lambda' \mathcal{F},$$

where  $\Lambda'$  is a diagonal unitary matrix.

We can write  $\sigma$  in eq. (14) as

$$\sigma = \begin{bmatrix} \mathcal{F}^\dagger & \mathbf{0} \\ \mathbf{0} & \mathcal{F}^\dagger \end{bmatrix} \begin{bmatrix} \Lambda & \mathbf{0} \\ \mathbf{0} & \Lambda' \end{bmatrix} \begin{bmatrix} \mathcal{F} & \mathbf{0} \\ \mathbf{0} & \mathcal{F} \end{bmatrix}.$$

---

<sup>3</sup>We realize that *velocity* is no longer an appropriate name for this form of steering.

We adopt the following notation for  $|v\rangle$ -controlled switch between matrices  $M$  and  $M'$  as

$$C^v(M, M') = \begin{bmatrix} M & \mathbf{0} \\ \mathbf{0} & M' \end{bmatrix}.$$

To be consistent with the previous section, we define  $C^v(M) := C^v(\mathbb{I}_N, M)$ , and  $C^{\bar{v}}(M) := C^v(M, \mathbb{I}_N)$ .

In the above notation,  $\sigma$  in Eq. (14) may be written

$$\sigma = (\mathbb{I}_v \otimes \mathcal{F}^\dagger) C^v(\Lambda, \Lambda') (\mathbb{I}_v \otimes \mathcal{F}), \quad (15)$$

where  $\mathbb{I}_v$  is the identity operator on the velocity space. Insofar as  $\Lambda, \Lambda'$  are efficiently implementable, and controllable by  $|v\rangle$  to switch between  $\Lambda$  and  $\Lambda'$ , we can efficiently implement a QW with its evolution based on  $C, C'$  using the QFT. Generally, if we can implement both  $C^v(\Lambda, \mathbb{I}_N) = C^{\bar{v}}(\Lambda)$  and  $C^v(\mathbb{I}_N, \Lambda') = C^v(\Lambda')$ , we can obtain  $C^v(\Lambda, \Lambda')$  as

$$C^v(\Lambda, \Lambda') = C^v(\Lambda, \mathbb{I}_N) C^v(\mathbb{I}_N, \Lambda') = C^{\bar{v}}(\Lambda) C^v(\Lambda') = C^v(\Lambda') C^{\bar{v}}(\Lambda).$$

The last equality is there as the controlled operations may be applied in either order. Let us re-examine the basic QW as an illustrative example of the setup of this section in a multi-qubit system and then consider the general case.

**3.1. Basic QW in a multi-qubit system revisited.** For the basic QW,  $C = \mathbf{X}$  and  $C' = \mathbf{X}^\top$ , with  $\Lambda = \Omega$  from eq. (13) and  $\Lambda' = \bar{\Omega}$ , the element-wise complex conjugate of  $\Omega$ ,

$$\bar{\Omega} = \bar{R}_n \otimes \bar{R}_{n-1} \otimes \bar{R}_{n-2} \otimes \cdots \otimes \bar{R}_1,$$

where  $R_j$  are as in eq. (12),

$$R_j = \begin{bmatrix} 1 & 0 \\ 0 & e^{2\pi i/2^j} \end{bmatrix},$$

and

$$\bar{R}_j = \begin{bmatrix} 1 & 0 \\ 0 & e^{-2\pi i/2^j} \end{bmatrix}.$$

We start with the standard controlled rotations (with  $|v\rangle$  as the control),

$$C_j^v(\bar{R}_j) = \begin{bmatrix} \mathbb{I}_2 & \mathbf{0} \\ \mathbf{0} & \bar{R}_j \end{bmatrix},$$

and

$$C_j^{\bar{v}}(R_j) = \begin{bmatrix} R_j & \mathbf{0} \\ \mathbf{0} & \mathbb{I}_2 \end{bmatrix}.$$

Note that

$$C_j^{\bar{v}}(R_j) = (X \otimes \mathbb{I}_2) C_j^v(R_j) (X \otimes \mathbb{I}_2) \quad (16)$$

Using these, we can construct

$$C^{\bar{v}}(\Omega) = \prod_{j=1}^n C_j^{\bar{v}}(R_j),$$

and

$$C^v(\bar{\Omega}) = \prod_{j=1}^n C_j^v(\bar{R}_j),$$

and thus

$$C^v(\Omega, \bar{\Omega}) = C^{\bar{v}}(\Omega) C^v(\bar{\Omega})$$

Substituting in (15), we get the propagation  $\sigma$  in the setup of this section,

$$\sigma = (\mathbb{I}_v \otimes \mathcal{F}^\dagger) C^v(\Omega, \bar{\Omega}) (\mathbb{I}_v \otimes \mathcal{F}).$$

This form of  $\sigma$  gives us another algorithm for the basic QW.

**3.2. Multi-qubit system: the general case.** Let us turn to the general unitary diagonal matrices  $\Lambda, \Lambda'$  of eq. (15) for the multi-qubit system. In [13], a method is described to efficiently implement multi-qubit diagonal unitary matrices, using CNOT gates and single qubit rotations of the form

$$R_\theta = e^{-i\frac{\theta}{2}Z} = \begin{bmatrix} e^{-i\frac{\theta}{2}} & 0 \\ 0 & e^{i\frac{\theta}{2}} \end{bmatrix}, \quad (17)$$

where

$$Z = \begin{bmatrix} 1 & 0 \\ 0 & -1 \end{bmatrix}.$$

The approximation in [13] uses partial Walsh-Fourier series. The circuit size depends on the approximation error  $\epsilon$  as  $O(1/\epsilon)$ , and is independent of  $n$  for large enough  $n$ . That implementation can be utilized with a simple modification to implement  $C^v(\Lambda)$  efficiently. Given an efficient circuit prescribed in [13] for the diagonal unitary matrix  $\Lambda$ , suppose that some qubit in the circuit has a rotation of the form  $R_\theta$  from eq. (17) applied to it. We replace this rotation with  $C^v(R_\theta)$ , the  $|v\rangle$ -controlled  $R_\theta$  applied to that qubit,

$$C^v(R_\theta) = \begin{bmatrix} \mathbb{I}_2 & \mathbf{0} \\ \mathbf{0} & R_\theta \end{bmatrix},$$

Substituting  $|v\rangle$ -controlled versions for all such rotations on all qubits would give us  $C^v(\Lambda)$ . In a similar manner, we can obtain  $C^{\bar{v}}(\Lambda)$  by substituting  $C^{\bar{v}}(R_\theta)$ , which can be constructed as in eq. (16) if necessary, for the rotations  $R_\theta$  that occur in the circuit for  $\Lambda$ . With  $C^{\bar{v}}(\Lambda)$  and  $C^v(\Lambda')$  thus constructed, we obtain

$$C^v(\Lambda, \Lambda') = C^{\bar{v}}(\Lambda) C^v(\Lambda') = C^v(\Lambda') C^{\bar{v}}(\Lambda).$$

We use this efficient implementation of  $C^v(\Lambda, \Lambda')$  and the  $2^n$  dimensional QFT implementation to obtain an efficient implementation of  $\sigma$  from eq. (15). An efficient QW algorithm for the given  $\Lambda, \Lambda'$  follows easily.

#### 4. SIMULATING QW WITH QFT BASED SHIFT ON QUANTUM COMPUTERS

We test the QW algorithm just described with the form of propagation from Section 2.1 and QFT based shift on three IBM quantum computers [16]: IBMQX2, IBMQX\_London and IBM\_16\_Melbourne, which are 5, 5 and 14 qubit machines respectively. The reader may find the machine gate and coupling maps in Appendix A Section A.1. IBM Qiskit [17] provides the API to access the computers and develop the python based code, transpile it, and run it.

The lattice sizes, walk step pairs in our simulations are (4, 1), (4, 2), and (8, 1) corresponding to  $n = 2, 3$  qubits. For all the simulations, we use the same scattering matrix

$$S = \frac{1}{\sqrt{2}} \begin{bmatrix} 1 & i \\ i & 1 \end{bmatrix}.$$

After initializing the walk joint velocity-position state, we run the algorithm for the given number of evolutionary steps. Then we measure the final state.

For each experiment, i.e., a set of lattice size, initial state, and steps of evolution, we execute the algorithm 1024 times (called “shots”) to generate a distribution on measured states.<sup>4</sup> The circuit is transpiled (compiled to quantum gates) using optimization level 3 of the transpiler prior to executing each experimental run. At this level, the transpiler takes in to account the noise properties and the connectivity of the device.

We repeat these runs, for each experiment and each machine, numerous times. We show the result from the run with the smallest  $\ell^1$  distance from the ideal distribution. Note that the  $\ell^1$  distance between two probability distributions  $P$  and  $Q$  over a finite, discrete variable  $i \in \mathcal{I}$  is

$$\ell^1(P, Q) = \frac{1}{2} \sum_{i \in \mathcal{I}} |P(i) - Q(i)|.$$

It takes values in  $[0, 1]$  range. For each experiment, we group together the plots of the distributions for all the machines, and also the ideal distribution that the QW state would have starting from the same state and after the same number of evolutionary steps. A table after each group of plots records the circuit size, the circuit depth, and the  $\ell^1$  distance between the ideal distribution and the ones shown. We point out that the circuits that give the distributions with the smallest  $\ell^1$  distance from the ideal do not always have the smallest transpiled size. We record the smallest circuit sizes in Appendix A Section A.3.

The first set of plots are for  $N = 4$  sites ( $n = 2$ ), and 1 step of walk evolution. Recall that the joint velocity-position state is  $|v, x\rangle$ . As a reminder, the joint velocity-position state is  $|v, x\rangle$ . For example, the state  $|011\rangle$  has  $|v\rangle = |0\rangle$ , and  $|x\rangle = |11\rangle$ . The initial walk state for this set of experiments is chosen to be  $|v, x\rangle = |010\rangle$ .

The ideal plot shows that the walk has moved both right and the left by 1 lattice point, having been scattered in both a left and a right moving component. The measured distributions show good agreement with the expected distribution for IBMQX2 and IBMQX\_London, but there are other states sampled as well. The distribution from IBM\_16\_Melbourne has stronger deviation from the ideal.<sup>5</sup> The circuit layouts for each case are in Appendix A Section A.2.

---

<sup>4</sup>For the terminology in this paper related to the IBM quantum computers, the reader might wish to look up IBM quantum computing website [16].

<sup>5</sup>We can speculate about the causes and sources of the deviations from the ideal. The circuit size and depth, gate noise, leakage, actual sequence of operations and decoherence, and other factors, are likely.

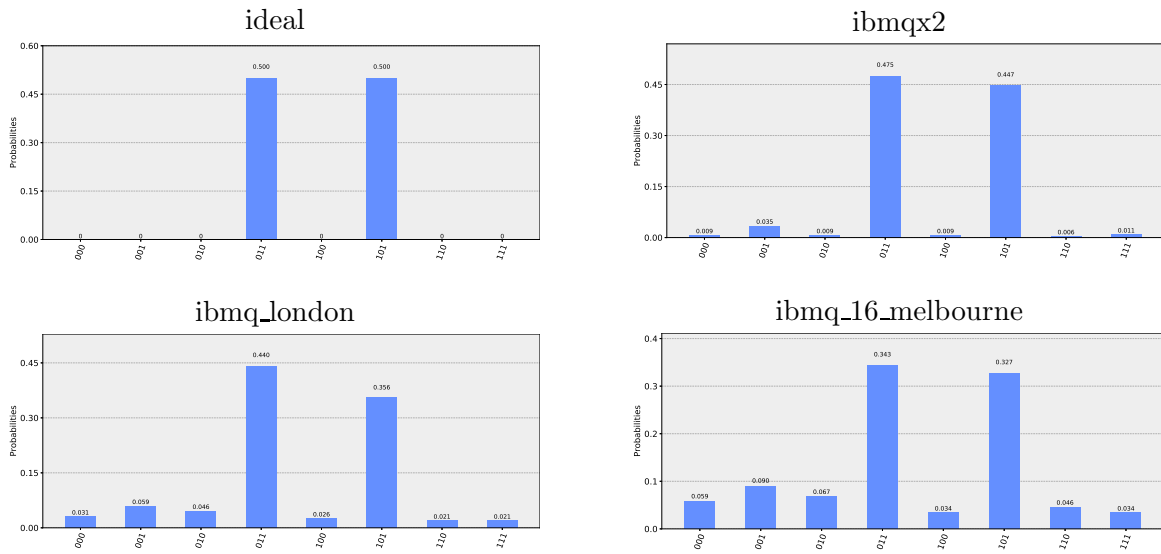


**Figure 6.** QFT based shift, 4 sites, 1 step

The table below summarizes the circuit size and depth, and the  $\ell^1$  distance of the measured distribution from the ideal distribution. It shows that different architectures transpile to different sizes (gate counts) and depths. Comparison with the gate coupling maps in Appendix A confirms the highest connectivity gate map, which is that of IBMQX2, corresponds to the lowest circuit size and depth, and the least deviation from the ideal distribution.

	(size , depth)	$\ell^1$ distance from ideal
ibmqx2	(11, 7)	0.0781
ibmq_london	(26, 18)	0.2031
ibmq_16_melbourne	(33, 21)	0.3301

**Table 1.** QFT based shift, 4 sites, 1 step

The next set of plots and the table are for  $N = 4$  sites ( $n = 2$ ), for 2 steps of walk evolution. Initial state of the walk is  $|v, x\rangle = |010\rangle$ .

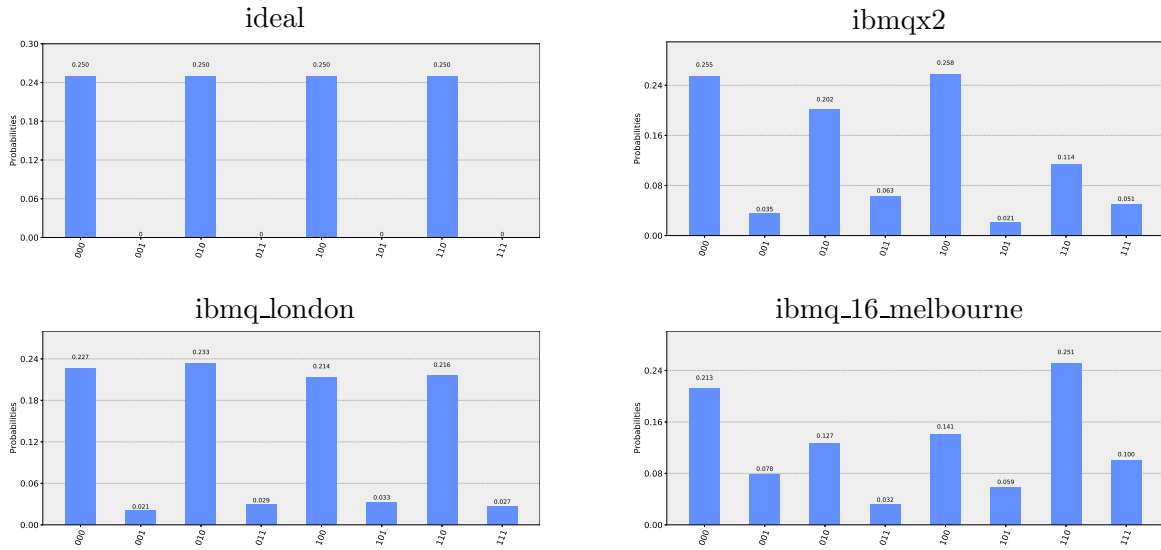


**Figure 7.** QFT based shift, 4 sites, 2 steps

The  $\ell^1$  distances in the table mimic the trend in the last section with generalized CNOT based shift. Interestingly, the values are lower for IBMQX-London and IBM16-Melbourne than those in the 1 step case.

	(size , depth)	$\ell^1$ distance from ideal
ibmqx2	(18, 11)	0.1836
ibmq_london	(55, 35)	0.1104
ibmq_16_melbourne	(57, 36)	0.2695

**Table 2.** QFT based shift, 4 sites, 2 steps

This last set of plots are for  $N = 8$  sites ( $n = 3$ ), and 1 step of walk evolution. Initial state of the walk is  $|v, x\rangle = |0010\rangle$ . While the distributions for IBMQX2 and IBMQX-London show reasonable agreement with the ideal, the distribution from IBM16-Melbourne is no longer recognizable as being a result of the quantum walk with discernible peaks at the correct states.

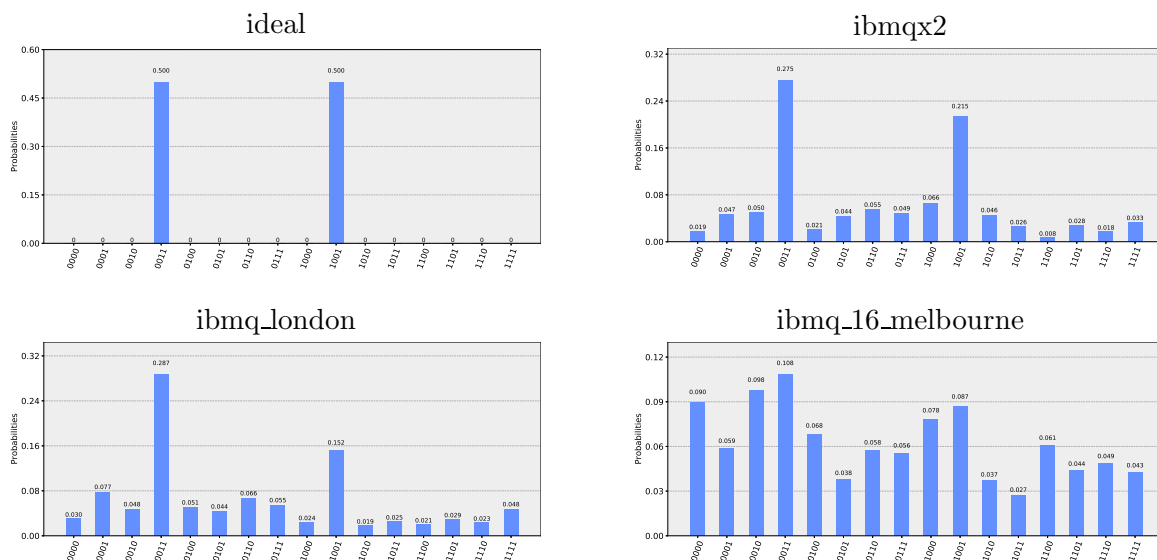


**Figure 8.** QFT based shift, 8 sites, 1 step

Overall, as apparent in the table below, the circuits are larger, respectively, than those encountered so far. The deviations from the ideal are more pronounced as well. IBM\_16\_Melbourne distribution is very distant from the ideal.

	(size , depth)	$\ell^1$ distance from ideal
ibmqx2	(62, 35)	0.5098
ibmq_london	(59, 38)	0.5605
ibmq_16_melbourne	(79, 50)	0.8047

**Table 3.** QFT based shift, 8 sites, 1 step

## 5. CONCLUSION

In this paper we have developed a QW algorithm that uses fewer resources by simplifying the structure of the controlled shift used to implement the propagation part of a QW. A single shift (increment) circuit suffices as opposed to both an increment and a decrement circuit that would usually be needed. The implementation allows any shift circuit, so that an optimized shift circuit dependent on the particular machine architecture may be substituted. In the NISQ regime where noise and decoherence adversely affect performance, this serves as an advantage. In comparison to a generalized CNOT based shift, a QFT based shift is generally an order of magnitude in  $n$ , the number of qubits, smaller and less deep and does not use ancilla qubits.

We examine and simulate the QW based on a QFT based shift. The algorithm was run on three IBM quantum computers: IBMQX2, IBMQX\_London and IBM\_16\_Melbourne, with 5, 5 and 14 qubit architectures respectively. We were able to simulate QW over small lattice sizes  $N = 4, 8$  ( $n = 2, 3$ ) and for 1 and 2 QW evolution steps, with reasonable results. We found that the higher connectivity architectures, like IBMQX2 and IBMQX\_London, generally perform better, though the transpiler optimizations and the machine architecture

and noise properties have a strong influence in determining the optimal circuit size and depth. We executed each run for 1024 shots, noting that a higher a number of shots would result in measurement distributions that are more accurate with respect to the machine behavior, especially for higher  $n$ .

We have implemented the simple QW based on a shift in this paper, but the method generalizes to circulant matrices (convolutions). The implementation of the latter would require care in implementing the controlled diagonal unitary matrices needed in propagation, for which we have indicated a method based on [13]. Future work could be directed toward QWs in higher dimensional lattices, aiming to characterize the QWs with spatial convolution that could have potential applications in quantum search, and in simulating models of physics. It could also seek to understand how the transpiler optimizations could be directed to improve the QW performance on specific architectures. In a similar vein, and more generally, quantum algorithms and simulation models could be adapted by mathematical structure to better meet the resource constraints of evolving quantum computers.

#### ACKNOWLEDGMENTS

The author would like to thank David Meyer for the ideas and discussions that motivated, and are partly represented in, this paper.

#### REFERENCES

- [1] P. Arrighi, G. Di Molfetta, I. Márquez-Martín, and A. Pérez, *Dirac equation as a quantum walk over the honeycomb and triangular lattices*, Phys. Rev. A **97** (2018), 062111. doi:10.1103/PhysRevA.97.062111.
- [2] D. W. Berry and A. M. Childs, *Black-box Hamiltonian simulation and unitary implementation*, Quantum Info. Comput. **12** (2012), 29–62. rintonpress.com/xxqic12/qic-12-12/0029-0062.eps.
- [3] F. Magniez, A. Nayak, J. Roland, and M. Santha, *Search via Quantum Walk*, SIAM J. Comput. **40** (2011), 142-164. doi:10.1145/1250790.1250874.
- [4] A. Schreiber, K. N. Cassemiro, V. Potoček, A. Gábris, P. J. Mosley, E. Andersson, I. Jex, and Ch. Silberhorn, *Photons Walking the Line: A Quantum Walk with Adjustable Coin Operations*, Physical Review Letters **104** (2010), no. 5, 050502. doi:10.1103/PhysRevLett.104.050502.
- [5] M. Broome, A. Fedrizzi, B. Lanyon, I. Kassal, A. Aspuru-Guzik, and A. White, *Discrete Single-Photon Quantum Walks with Tunable Decoherence*, Phys. Rev. Lett. **104** (2010), 153602. doi:10.1103/PhysRevLett.104.153602.
- [6] S. Venegas-Andraca, *Quantum walks: a comprehensive review*, Quant. Inf. Proc. **11** (2012), 1015–1106. doi.org/10.1007/s11128-012-0432-5.
- [7] J. Preskill, *Quantum Computing in the NISQ era and beyond*, Quantum **2** (2018), 79. doi:10.22331/q-2018-08-06-79.
- [8] D. A. Meyer, *From quantum cellular automata to quantum lattice gases*, Journal of Statistical Physics **85** (1996), 551–574. doi:10.1007/BF02199356.
- [9] G. Golub and C. Van Loan, *Matrix Computations: 4<sup>th</sup> Edition*, Johns Hopkins Studies in the Mathematical Sciences, Johns Hopkins University Press, Baltimore, MD, 2013.
- [10] B. Douglas and J. Wang, *Efficient quantum circuit implementation of quantum walks*, Phys. Rev. A **79** (2009), 052335. doi:10.1103/PhysRevA.79.052335.
- [11] P. Shor, *Polynomial-Time Algorithms for Prime Factorization and Discrete Logarithms on a Quantum Computer*, SIAM Journal on Computing **26** (1997), no. 5, 1484–1509. doi:10.1137/S0097539795293172.
- [12] M. Nielsen and I. Chuang, *Quantum Computation and Quantum Information: 10th Anniversary Edition*, Cambridge University Press, New York, 2010. doi:10.1017/CBO9780511976667.
- [13] J. Welch, D. Greenbaum, S. Mostame, and A. Aspuru-Guzik, *Efficient quantum circuits for diagonal unitaries without ancillas*, New Journal of Physics **16** (2014), no. 3, 033040. doi:10.1088/1367-2630/16/3/033040.



- [14] A. Barenco, C. Bennett, R. Cleve, D. DiVincenzo, N. Margolus, P. Shor, T. Sleator, J. Smolin, and H. Weinfurter, *Elementary gates for quantum computation*, Phys. Rev. A **52** (1995), 3457–3467. doi:10.1103/PhysRevA.52.3457.
- [15] M. Saeedi and M. Pedram, *Linear-depth quantum circuits for  $n$ -qubit Toffoli gates with no ancilla*, Phys. Rev. A **87** (2013), 062318. doi:10.1103/PhysRevA.87.062318.
- [16] *IBM Quantum Experience*, 2019. url:quantum-computing.ibm.com.
- [17] *Qiskit: An Open-source Framework for Quantum Computing*, 2019. url:qiskit.org.

## APPENDIX A. COUPLING MAPS, LAYOUTS AND SMALLEST TRANPILED CIRCUIT SIZES

A.1. **Coupling maps.** These are the IBM quantum computer coupling maps for the machines in this paper. The directional arrows show source-target pair for controlled operations. Arrows in both directions mean both qubits can serve as the control and target.

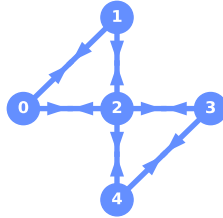


**Figure 9.** ibmqx2 coupling map

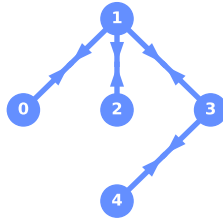


**Figure 10.** ibmq\_london coupling map

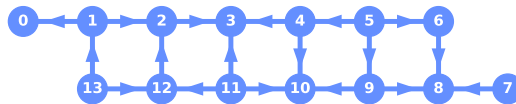


**Figure 11.** ibmq\_16\_melbourne coupling map

**A.2. Layouts for QFT based shift.** Here we show the layout maps for each of the experiments with QFT based shift. The qubits and couplings in black are involved in the respective circuit.

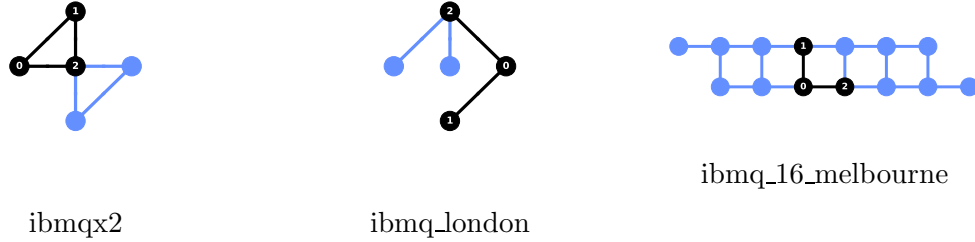


**Figure 12.** QFT based shift, 4 sites, 1 step.

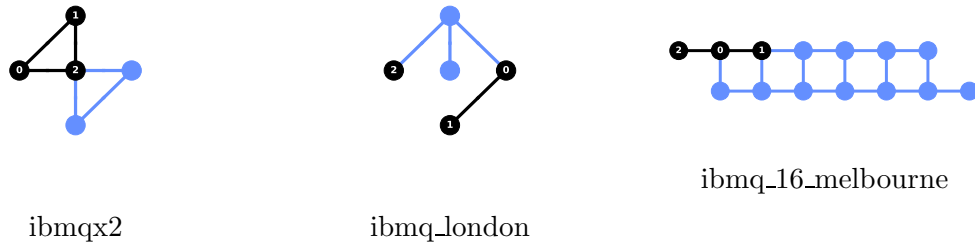


**Figure 13.** QFT based shift, 4 sites, 2 steps.

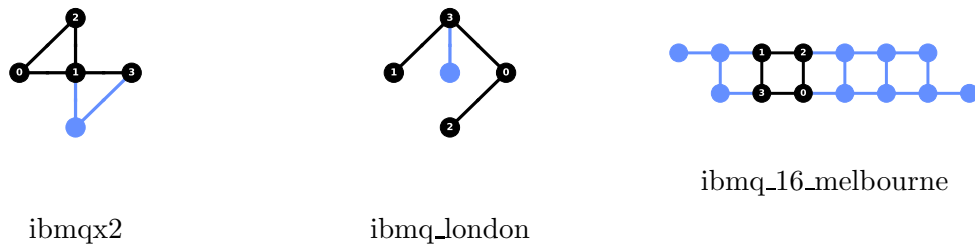


**Figure 14.** QFT based shift, 8 sites, 1 step.

**A.3. Smallest transpiled circuit sizes.** The smallest circuit sizes that were obtained during simulations are given below for the respective experiments. These are not always the same as the circuits that gave the least  $\ell^1$  distance from the ideal distribution shown in the main body of the paper.

	(size , depth)
ibmqx2	(11, 7)
ibmq_london	(21, 15)
ibmq_16_melbourne	(25, 16)

**Table 4.** QFT based shift, 4 sites, 1 step

	(size , depth)
ibmqx2	(18, 11)
ibmq_london	(38, 29)
ibmq_16_melbourne	(48, 30)

**Table 5.** QFT based shift, 4 sites, 2 steps

	(size , depth)
ibmqx2	(47, 33)
ibmq_london	(59, 38)
ibmq_16_melbourne	(78, 45)

**Table 6.** QFT based shift, 8 sites, 1 step